Arnold, K., Pratsch, L., & Gawrisch, K. (1983) *Biochim. Biophys. Acta 728*, 121–128.
Arvidson, G., Brentel, I., Khan, A., Lindblom, G., & Fontell, K. (1985) *Eur. J. Biochem. 152*, 753–759.
Boni, L. T., Stewart, T. P., Alderfer, J. L., & Hui, S. W. (1981) *J. Membr. Biol. 62*, 71–77.
Eriksson, P.-O., Lindblom, G., & Arvidson, G. (1985) *J. Phys. Chem. 89*, 1050–1053.
Fontell, K., Fox, K., & Hansson, E. (1985) *Mol. Cryst. Liq. Cryst., Lett. Sect. 1*, 9–17.
Hauser, H., Pascher, I., & Sundell, S. (1980) *J. Mol. Biol. 137*, 249–264.
Huang, C.-H., Lapides, J. R., & Levin, I. W. (1982) *J. Am. Chem. Soc. 104*, 5926–5930.
Lucy, J. A. (1984) *Ciba Found. Symp. 103*, 28–39.
Luzzati, V. (1968) in *Biological Membranes* (Chapman, D., Ed.) Vol. 1, pp 71–123, Academic Press, London.
MacDonald, R. I. (1985) *Biochemistry 24*, 4058–4066.
Mariani, P., Luzzati, V., & Delacroix, H. (1988) *J. Mol. Biol. 204*, 165–189.
Mattai, J., & Shipley, G. G. (1986) *Biochim. Biophys. Acta 859*, 257–265.
Powell, G. L., & Marsh, D. (1985) *Biochemistry 24*, 2902–2908.
Seddon, J. M., Cevc, G., Kaye, R. D., & Marsh, D. (1984) *Biochemistry 23*, 2634–2644.
Seelig, J. (1978) *Biochim. Biophys. Acta 515*, 105–140.
Tilcock, C. P. S., & Fisher, D. (1979) *Biochim. Biophys. Acta 557*, 53–61.
Tilcock, C. P. S., Cullis, P. R., Hope, M. J., & Gruner, S. M. (1986) *Biochemistry 25*, 816–822.
van Echteld, C. J. A., de Kruijff, B., & de Gier, J. (1980) *Biochim. Biophys. Acta 595*, 71–81.
van Echteld, C. J. A., de Kruijff, B., Mandersloot, J. G., & de Gier, J. (1981) *Biochim. Biophys. Acta 649*, 211–220.
Wu, W.-G., & Huang, C.-H. (1983) *Biochemistry 22*, 5068–5073.
Wu, W.-G., Huang, C.-H., Conley, T. G., Martin, R. B., & Levin, I. W. (1982) *Biochemistry 21*, 5957–5961.

NMR Studies of Exocyclic 1,N^2-Propanodeoxyguanosine Adducts (X) opposite Purines in DNA Duplexes: Protonated X(syn)·A(anti) Pairing (Acidic pH) and X(syn)·G(anti) Pairing (Neutral pH) at the Lesion Site†

Michael Kouchakdjian,‡ Edmund Marinelli,§ Xiaolian Gao,‡ Francis Johnson,§ Arthur Grollman,*,§ and Dinshaw Patel*,‡

Department of Biochemistry and Molecular Biophysics, College of Physicians and Surgeons, Columbia University, New York, New York 10032, and Department of Pharmacological Sciences, State University of New York at Stony Brook, Stony Brook, New York 11794

Received October 31, 1988; Revised Manuscript Received March 6, 1989

ABSTRACT: Proton and phosphorus two-dimensional NMR studies are reported for the complementary d(C1-A2-T3-G4-*X5*-G6-T7-A8-C9)·d(G10-T11-A12-C13-*A14*-C15-A16-T17-G18) nonanucleotide duplex (designated X·A 9-mer) that contains a 1,N^2-propanodeoxyguanosine exocyclic adduct, X5, opposite deoxyadenosine A14 in the center of the helix. The NMR studies detect a pH-dependent conformational transition; this paper focuses on the structure present at pH 5.8. The two-dimensional NOESY studies of the X·A 9-mer duplex in H_2O and D_2O solution establish that X5 adopts a syn orientation while A14 adopts an anti orientation about the glycosidic bond at the lesion site. The large downfield shift of the amino protons of A14 demonstrates protonation of the deoxyadenosine base at pH 5.8 such that the protonated X5(syn)·A14(anti) pair is stabilized by two hydrogen bonds at low pH. At pH 5.8, the observed NOE between the H8 proton of X5 and the H2 proton of A14 in the X·A 9-mer duplex demonstrates unequivocally the formation of the protonated X5(syn)·A14(anti) pair. The 1,N^2-propano bridge of X5(syn) is located in the major groove. Selective NOEs from the exocyclic methylene protons of X5 to the major groove H8 proton of flanking G4 but not G6 of the G4-X5-G6 segment provide additional structural constraints on the local conformation at the lesion site. A perturbation in the phosphodiester backbone is detected at the C13-A14 phosphorus located at the lesion site by ^{31}P NMR spectroscopy. The two-dimensional NMR studies have been extended to the related complementary X·G 9-mer duplex that contains a central X5·G14 lesion in a sequence that is otherwise identical with the X·A 9-mer duplex. The NMR experimental parameters are consistent with formation of a pH-independent X5(syn)·G14(anti) pair stabilized by two hydrogen bonds with the 1,N^2-propano exocyclic adduct of X5(syn) located in the major groove.

Since the original paper by Shapiro et al. (1969), a number of compounds have been reported to form exocyclic nucleic acid adducts with DNA [reviewed in Singer and Barsch (1986), Singer and Grunberger (1983), and Basu and Essigmann (1988)]. Cyclic derivatives may affect base pairing, and it has been suggested that these structures play an important role in mutagenesis and carcinogenesis.

Acrolein reacts readily with deoxyguanosine to form three cyclic adducts (Chung et al., 1984). The reaction of this

†This research was supported by a Columbia University Faculty Start-Up Grant to D.J.P. and NIH Grants ES-04068 and CA-17395 to A.P.G.
‡Columbia University.
§State University of New York at Stony Brook.

0006-2960/89/0428-5647$01.50/0

α,β-unsaturated carbonyl compound involves Michael's addition to the N-1 and N-2 positions of the base, followed by ring closure. One of these adducts (**1**) was also obtained following enzymatic hydrolysis of calf thymus DNA treated with acrolein under physiological conditions (Chung et al., 1984).

The presence of a hydroxyl group at either the 1- or 3-position of the propano bridge introduces a degree of chemical instability and gives rise at each site to diastereoisomers. These complications are avoided by omission of the hydroxyl group as in structure **2** resulting in a stable 1,N^2-propanodeoxyguanosine exocyclic adduct. The synthesis of oligodeoxynucleotides containing **2** can readily be accomplished by solid-state methods. We are using these modified oligomers to study the molecular structure and biological function of exocyclic adducts derived from reactions of α,β-unsaturated carbonyl compounds with deoxyguanosine. Our approach parallels that taken in previous studies on abasic sites in DNA (Takeshita et al., 1987; Kalnik et al., 1988) in which a highly stable anhydroribotol moiety was used as a model for the cyclic form of the naturally occurring deoxyribose.

Nuclear magnetic resonance offers spectral resolution at the level of individual base pairs [see reviews by Reid (1987), Patel et al. (1987), and van de Ven and Hilbers (1988)] and is the method of choice for investigations of nucleic acid solution structure and dynamics. The NMR studies reported in this paper focus on 1,N^2-propanodeoxyguanosine (**2**) (designated X), embedded in the center of DNA oligonucleotide duplexes. Experiments were performed by using the complementary nonadeoxynucleotide **3** (designated X·A 9-mer), which contains

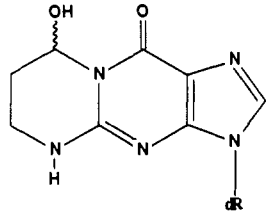

1

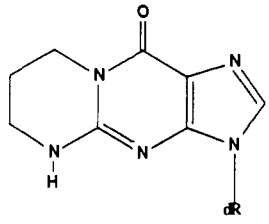

2

C1-A2-T3-G4-X5-G6-T7-A8-C9
G18-T17-A16-C15-A14-C13-A12-T11-G10

3

C1-A2-T3-G4-X5-G6-T7-A8-C9
G18-T17-A16-C15-G14-C13-A12-T11-G10

4

the exocyclic adduct X located opposite deoxyadenosine, and the related complementary nonadeoxynucleotide **4** (designated X·G 9-mer). The results demonstrate that a stable right-handed duplex DNA structure forms at pH 5.8 with 1,N^2-propanodeoxyguanosine adopting the syn conformation and the deoxyadenosine and deoxyguanosine residues located opposite the lesion in the anti conformation.

Experimental Procedures

Oligonucleotide Synthesis. 1,N^2-(1,3-Propano)-2′-deoxyguanosine (**2**) was prepared most easily by treatment of 2′-deoxyguanosine with 1,3-dibromopropane in dimethyl sulfoxide, the experimental details of which will be disclosed in a separate publication (E. Marinelli and F. Johnson, unpublished results). The modified deoxynucleoside was purified by silica gel flash chromatography and was demonstrated to be homogeneous by reverse-phase HPLC analysis (Waters, 10-μm C-18 Resolve Radial-Pak column; 0–40% acetonitrile into 0.05 M triethylamine acetate (TEAA) over 20 min, flow rate 2.0 mL/min, retention time 9.93 min) and found to be free of 2′-deoxyguanosine (detection limit, 0.2 area %). The one- and two-dimensional proton NMR data, UV spectra and both low- and high-resolution mass spectroscopy data are all found to be consistent with the stated structure. The 5′-*O*-(dimethyoxytrityl) (DMT) ether of **2** and the further derived 3′-*O*-(β-cyanoethyl *N*,*N*-diisopropylphosphoramidite) were prepared by standard methods and displayed spectral data that confirmed their structures.

The desired oligodeoxynucleotides were assembled on 5 μmol of resin by employing a Du Pont Coder 300 automated DNA synthesizer, the above phosphoramidite being added manually in a normal coupling reaction. The resulting oligodeoxynucleotides was then simultaneously removed from the resin and deprotected by the standard ammonia treatment. The resulting oligomer having a terminal 5′-*O*-DMT ether residue was purified by using a 7.8 mm × 30 cm semipreparative C-18 Waters μBondapak reverse-phase column. The desired material was eluted over 10 min with a gradient of 20–40% acetonitrile into 0.10 M TEAA at a flow rate of 2.0 mL/min. Under these conditions the retention time of the DMT–DNA is 13.29 min. Detritylation was then accomplished by means of 20% aqueous acetic acid at 25 °C for 30 min. Further purification of the modified DNA oligomer was carried out by again using the Waters semipreparative column. Elution occurred over 10 min with a gradient of 10–20% acetonitrile into 0.10 M TEAA at 2.0 mL/min; retention time was 11.25 min. The oligomer migrated as a single band when subjected to electrophoresis in a buffer (pH 8.3) composed of 7 M urea, 100 mM Tris–borate, and 10 mM EDTA.

Sample Preparation. NMR experiments were performed on 250 A_{260} units of the X·A 9-mer duplex and 200 A_{260} units of the X·G 9-mer duplex. Both DNA preparations contain 0.1 M NaCl, 10 mM phosphate, and 1 mM EDTA in 0.4 mL of either 100% D_2O or 90% H_2O/10% D_2O (v/v). The pH values in D_2O are uncorrected pH meter readings.

NMR Experiments. Proton NMR experiments were recorded on a Bruker AM 500 spectrometer. Proton chemical shifts are referenced relative to external TSP. One- and two-dimensional phosphorus experiments were performed at 121.5 MHz on a Bruker AM 300 spectrometer. Phosphorus chemical shifts are referenced relative to internal trimethyl phosphate (TMP).

One-dimensional NMR spectra of both the X·A 9-mer and the X·G 9-mer in H_2O were collected by using a jump and return ($90y$, τ, $90 - y$) pulse for solvent suppression. One-dimensional difference NOE experiments were conducted by using a 1–1 H_2O suppression pulse (Hore, 1983). The carrier frequency was shifted 6000 Hz downfield from the H_2O resonance, and the 1–1 delay was optimized for solvent suppression. Data were collected over a spectral width of 20 000 Hz by using 2048 complex data points with a 0.4-s repetition delay. Resonances were irradiated for 400 ms with the decoupler channel. The FIDs were subtracted after an exponential line broadening of 5 Hz was applied and were Fourier transformed to obtain the NOE difference spectra.

Two-dimensional phase-sensitive NOESY spectra in H_2O were recorded by using a jump and return ($90y$, τ, $90 - y$) detection pulse. Preparation and mixing pulses were 70° hard pulses, and the mixing time was 120 ms (1.0-s repetition delay). The carrier frequency was centered on the H_2O signal, and the waiting time was optimized so that the imino and aromatic protons were equally excited. The time domain data sets consist of 1024 complex data points over a spectral width of 10000 Hz in the t_2 dimension. Each of the 256 t_1 increments collected consisted of 256 scans. The free induction decays were apodized with a 90° shifted sine bell function zeroed to the 1024th point in the t_2 dimension and to the 256th point in t_1. Each dimension was base-line corrected with a fifth-order polynomial base-line fitting routine following Fourier transformation.

Two-dimensional phase-sensitive NOESY spectra were collected on both the X·A 9-mer and X·G 9-mer duplexes in D_2O buffer with a repetition delay of 1.5 s and a spectral width of 5000 Hz. A 250-ms mixing time was used for the X·A 9-mer, while a mixing time of 300 ms was used for the X·G duplex. The carrier frequency was positioned on the residual HOD resonance, and this resonance was presaturated by using the decoupler channel. The data sets were collected with 256 t_1 increments using 1024 complex data points in the t_2 dimension and 32 scans per t_1 increment. The free induction decays were apodized with a 90° shifted sine bell function at the 1024th point in the t_2 dimension and at the 256th point in the t_1 dimension and were Fourier transformed in both dimensions.

The phase-sensitive two-dimensional ^{31}P–^1H heteronuclear correlation experiment of the X·A 9-mer duplex in D_2O utilized a MLEV-17 composite pulse scheme that achieves a net magnetization transfer among protons via a homonuclear Hartmann–Hahn (HOHAHA) type cross-polarization (M. Zagorski, unpublished results). This net magnetization transfer is then relayed to the ^{31}P atoms via an INEPT sequence. The carrier frequency was placed at the center of both ^{31}P and ^1H dimensions. The time domain data sets were accumulated over a spectral width of 314 Hz by using 512 data points in t_2 and a spectral width of 1400 Hz in t_1. A total of 65 t_1 increments were collected with a 1.7-s repetition delay, 30-ms spin lock time, and 1024 scans per increment. Both dimensions were zero filled to 1024 complex data points and were apodized with a 90° shifted sine bell function, and the t_1 dimension was line broadened by 2 Hz prior to Fourier transformation.

The one- and two-dimensional data sets were processed by using FTNMR software on a MicroVAXII. Two-dimensional data sets were processed with the t_1 noise reduction routine of Otting et al. (1985).

Results

The numbering system of the complementary nonadeoxynucleotide strands of the X·A 9-mer and X·G 9-mer duplexes are shown in **3** and **4**, respectively.

X·A 9-mer

pH-Dependent Conformational Transition. The nonexchangeable proton NMR spectra (5.0–9.0 ppm) of the X·A 9-mer in D_2O buffer, 15 °C at pH 5.8 and pH 8.9, exhibit narrow resonances with different chemical shifts indicative of a pH-dependent conformational transition of the X·A 9-mer duplex. At intermediate pH values, both forms can be detected in slow exchange. The NMR results presented below focus on the spectral data for the X·A 9-mer duplex at pH 5.8, while the corresponding spectral data and their interpretation at pH 8.9 will be reported in a subsequent publication.

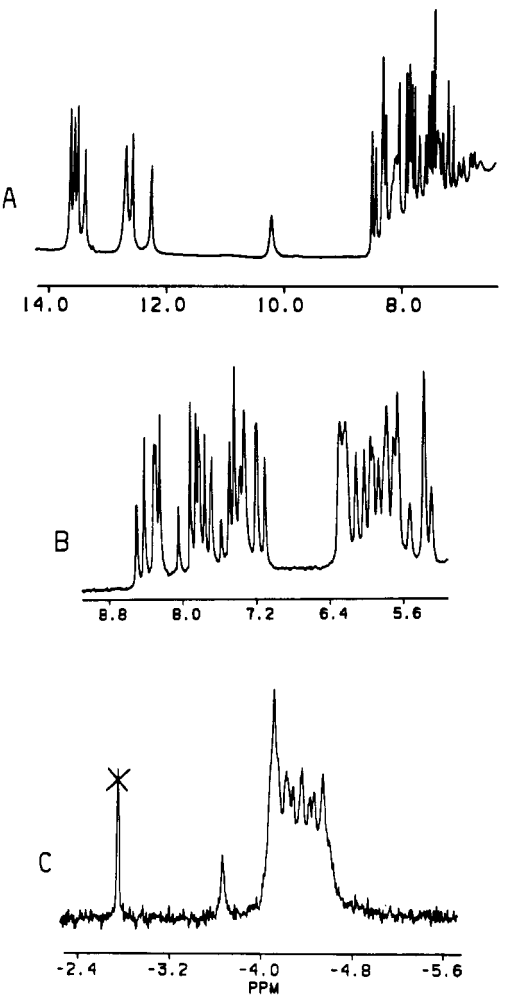

FIGURE 1: (A) Exchangeable 500-MHz proton (6.0–14.0 ppm), (B) nonexchangeable 500-MHz proton (5.0–9.0 ppm), and (C) proton-decoupled 121-MHz phosphorus (−2.4 to −5.6 ppm) spectra of the X·A 9-mer duplex in 0.1 M NaCl, 10 mM phosphate, aqueous solution, pH 5.8 at 15 °C.

Insertion of the exocyclic adduct **2** in the center of the X·A 9-mer duplex **3** results in the destabilization of the helix. A similar destabilization was detected with complementary 9-mer duplexes containing a central abasic site (Kalnik et al., 1988). Accordingly, the NMR studies were performed at temperatures ranging from 5 to 15 °C at which the duplex is intact.

Exchangeable Protons. The exchangeable proton spectrum (6.0–14.0 ppm) of the X·A 9-mer duplex in H_2O buffer (0.1 M NaCl, 10 mM phosphate), pH 5.8 at 15 °C, is plotted in Figure 1A. The exchangeable imino protons (deoxyguanosine N1H and thymidine N3H) resonate between 12.0 and 14.0 ppm, while the exchangeable amino protons and nonexchangeable base protons resonate between 6.5 and 8.5 ppm. An additional exchangeable resonance is detected at 10.18 ppm in Figure 1A.

The phase-sensitive NOESY spectrum (120-ms mixing time) of the X·A 9-mer duplex in H_2O buffer, pH 5.8 at 15 °C, is shown as a contour plot in Figure 2A. The box B region in Figure 2A establishes distance connectivities between the 12.0–14.0 ppm imino protons and the 5.0–8.5 ppm base and amino protons. An expanded plot of this region is presented in Figure 2B. The observed NOEs between the thymidine imino and deoxyadenosine H2 protons (peaks C–F, Figure 2B) and between the deoxyguanosine imino and hydrogen-bonded (peaks G and I, Figure 2B) and exposed (peaks H and J, Figure 2B) deoxycytidine amino protons establish the align-

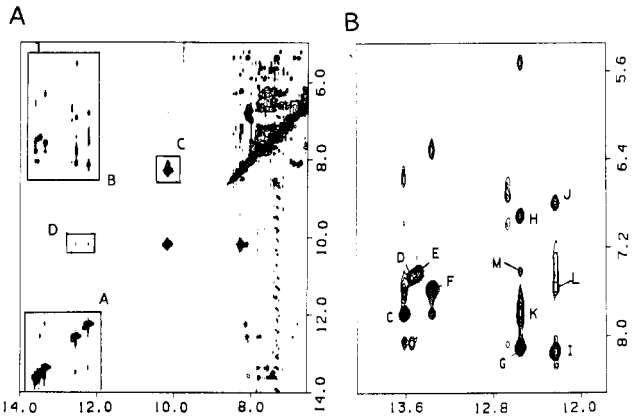

FIGURE 2: Phase-sensitive NOESY spectra (mixing time 120 ms) of the X·A 9-mer duplex in 0.1 M NaCl, 10 mM phosphate solution, and H_2O, pH 5.8 at 15 °C. (A) Cross peaks establishing connectivities in the symmetrical 5.0–14.0 ppm range. (B) Cross peaks establishing connectivities between the imino protons (12.0–14.0 ppm) and the base and amino protons (5.4–8.4 ppm). The cross peaks C–M are discussed in the text.

ment of bases across the A·T and G·C pairs in the X·A 9-mer duplex.

The imino protons can be assigned to specific base pairs in the X·A 9-mer duplex on the basis of NOEs between these protons and the protons on adjacent base pairs. Specifically, the imino proton of G4 in the G4·C15 pair exhibits an NOE to the imino proton of T3 (cross peak in box A, Figure 2A) and the H2 proton of A16 (peak L, Figure 2B) of the flanking T3·A16 base pair in one direction and the hydrogen-bonded amino proton of A14 (right peak in box D, Figure 2A) in the other direction. Similarly, the imino proton of G6 in the G6·C13 pair exhibits an NOE to the imino proton of T7 (cross peak in box A, Figure 2A) and the H2 proton of A12 (peak M, Figure 2B) of the flanking T7·A12 base pair in one direction and the hydrogen-bonded amino proton of A14 (left peak in box D, Figure 2A) in the other direction.

The chemical shifts of the imino and amino protons and deoxyadenosine H2 protons in the X·A 9-mer duplex in H_2O buffer at 15 °C are listed in Table I.

We detect a strong cross peak between exchangeable protons at 10.18 and 8.28 ppm (box C, Figure 2A) in the NOESY spectrum of the X·A 9-mer duplex. These protons must originate from geminal NH_2 protons and are assigned to the hydrogen-bonded (10.18 ppm) and exposed (8.28 ppm) amino protons of A14 at the X5·A14 lesion site. These assignments are based on the observed NOEs between the 10.18 ppm proton and the imino protons in the flanking G4·C15 and G6·C13 base pairs (box D, Figure 2A) in the X·A 9-mer duplex. This assignment is confirmed by the one-dimensional NOE difference experiments.

Nonexchangeable Protons. The nonexchangeable proton NMR spectrum (5.0–9.0 ppm) of the X·A 9-mer in D_2O buffer, pH 5.8 at 15 °C, is plotted in Figure 1B. The phase-sensitive NOESY spectrum (250-ms mixing time) of the X·A 9-mer duplex in D_2O buffer, pH 5.8 at 15 °C, is displayed as a contour plot (symmetrical 1.0–9.0 ppm) in Figure 3A. The cross peaks are well resolved, and we focus below on data enclosed in the boxes A–D in this NOESY spectrum.

Box A in Figure 3A establishes distance connectivities between the base protons (7.0–8.6 ppm) and the sugar H1′ and deoxycytidine H5 protons (5.0–6.4 ppm) with expanded plots of this region presented in duplicate in Figure 4. The base (purine H8 and pyrimidine H6) protons exhibit NOEs to their own and 5′-flanking sugar H1′ protons characteristic of right-handed duplexes (Hare et al., 1983), permitting the chain to be traced from C1 to C9 in the modified strand (Figure 4A) and from G10 to G18 in the unmodified strand (Figure 4B).

The NOE cross peak between the H8 proton of X5 and its own sugar H1′ proton is strong (peak X5, Figure 4A), whereas the NOE to the H1′ proton of G4 in the 5′-direction is absent. By contrast, the H8 proton of A14 exhibits NOEs to its own sugar H1′ proton (peak A14, Figure 4B) and to the H1′ proton of C13 in the 5′-direction.

Stacked plots of this expanded NOESY region of the X·A 9-mer for data collected at 250- and 50-ms mixing times are plotted in parts A and B of Figure 5, respectively. The intensities of the base to its own sugar H1′ proton NOEs for X5 (peak X5 in Figure 5) and A14 (peak A14 in Figure 5) are

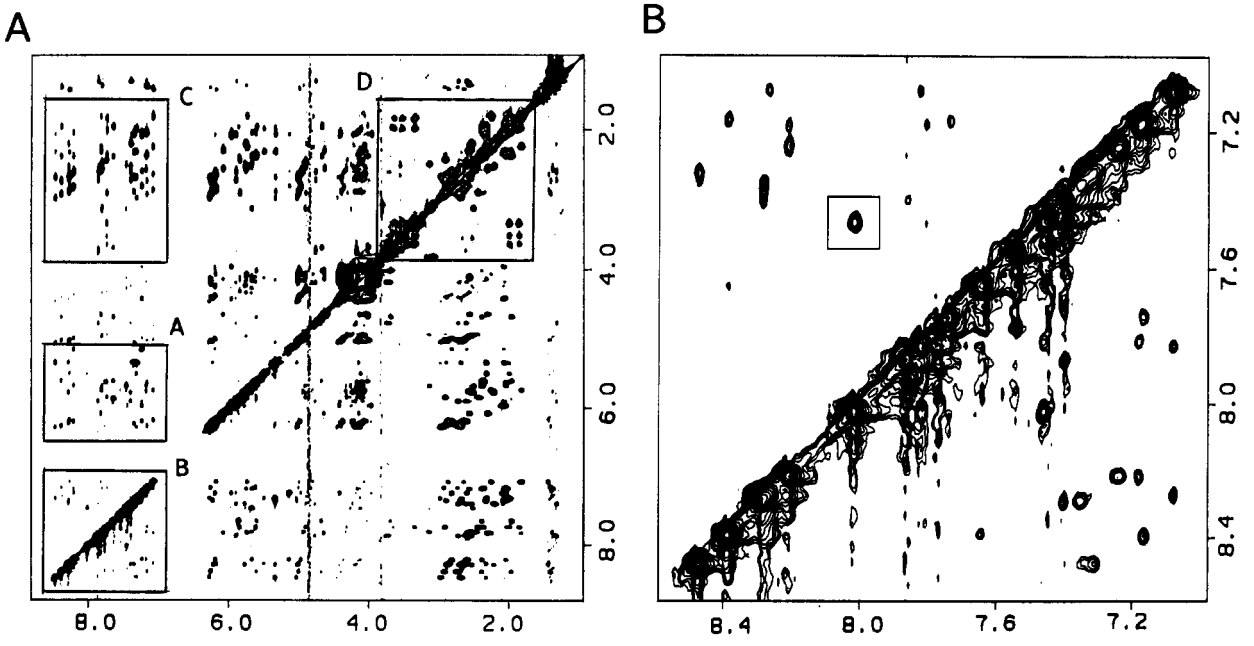

FIGURE 3: Phase-sensitive NOESY spectra (mixing time 250 ms) of the X·A 9-mer duplex in 0.1 M NaCl, 10 mM phosphate, and D_2O, pH 5.8 at 15 °C. (A) Cross peaks establishing connectivities in the symmetrical 1.0–9.0 ppm region. (B) Cross peaks establishing connectivities between the base protons in the symmetrical 7.0–8.6 ppm region.

Table I: Proton Chemical Shifts in X·A 9-mer Duplex, pH 5.8, 15 °C

	exchangeable proton chemical shifts (ppm)					
base pair	T-H3	G-H1	C-H4b	C-H4e	A-H2	A-H6
C1·G18		12.67	8.05	6.99		
A2·T17	13.61				7.80	7.58, 6.57
T3·A16	13.36				7.58	7.61, 6.13
G4·C15		12.23	8.14	6.79		
X5·A14						10.18, 8.28
G6·C13		12.55	8.11	6.92		
T7·A12	13.49				7.43	
A8·T11	13.54				7.48	
C9·G10		12.67	8.09	6.74		

	nonexchangeable proton chemical shifts (ppm)							
	H8	H2	H6	H5/CH_3	H1′	H2′,H2″	H3′	H4′
C1			7.65	5.87	5.61	1.97, 2.39	4.67	4.02
A2	8.39	7.77			6.26	2.73, 2.93	5.01	4.39
T3			7.17	1.41	5.62	2.05, 2.36		4.17
G4	7.74				5.84	2.44, 2.91	4.92	4.31
X5	7.46				5.67	2.51, 3.14	4.93	4.26
G6	7.81				5.75	2.26, 2.58	4.94	4.33
T7			7.18	1.38	5.67	2.05, 2.39		
A8	8.21	7.44			6.20	2.61, 2.82	4.97	4.36
C9			7.24	5.14	5.97	2.05, 2.10		4.42
G10	7.86				5.90	2.62, 2.73	4.75	
T11			7.40	1.32	5.78	2.21, 2.54	4.91	4.23
A12	8.28	7.39			6.23	2.69, 2.89	5.03	4.41
C13			7.35	5.34	5.34	2.07, 2.33		4.15
A14	8.47	8.02			6.29	2.69, 2.98	5.04	4.45
C15			7.32	5.34	5.50	1.99, 2.33		4.12
A16	8.27	7.54			6.18	2.65, 2.86	5.01	
T17			7.08	1.44	5.74	1.82, 2.26	4.78	4.07
G18	7.82				6.08	2.31, 2.57	4.64	4.14

compared relative to the intensities of the NOEs between the H6 and H5 (fixed interproton separation of 2.45 Å) protons for the deoxycytidines (designated C* in Figure 5). The peak labeled X5 is approximately 0.7 the intensity of the C9* peak, whereas the peak labeled A14 cannot be detected at the short mixing time (Figure 5B).

Box B in Figure 3A establishes distance connectivities between base protons in the symmetrical 7.0–8.6 ppm region. An expanded plot of this region is presented in Figure 3B. A cross peak is detected between the 7.46 ppm H8 proton of X5 and the 8.02 ppm H2 proton of A14 (boxed peak in Figure 3B), and this places constraints on the alignment of bases at the X5·A14 lesion site.

Box C of Figure 3A establishes distance connectivities between the base protons (7.0–8.6 ppm) and the sugar H2′,2″ protons (1.6–4.0 ppm) with an expanded plot of this region presented in Figure 6A. We detect NOEs from the H8 proton of A14 to its own H2′,2″ protons (linked by a line labeled A14, Figure 6A) and to the H2′,2″ protons of C13 in the 5′-direction, while NOEs are detected from the H8 proton of X5 to its own H2′,2″ protons (linked by a line labeled X5, Figure 6A) but not to the H2′,2″ protons of G4 in the 5′-direction.

The base and sugar proton chemical shifts of the X·A 9-mer at 15 °C are listed in Table I and are based on the above assignment procedures as well as an analysis of the remaining regions of the NOESY spectrum in Figure 3A.

Box D in Figure 3A establishes distance connectivities between sugar H2′,2″ protons and between the methylene protons of the exocyclic ring in the symmetrical 1.6–4.0 ppm region. An expanded plot of this region is presented in Figure 6B. We detect NOEs between adjacent exocyclic CH_2 protons, permitting assignment of the 1.85 and 2.00 ppm resonances to the central CH_2 protons, and the 3.35 (superpositioned), 3.53, and the 3.65 ppm resonances to the flanking CH_2 protons (Figure 6B). All CH_2 protons of the exocyclic ring exhibit

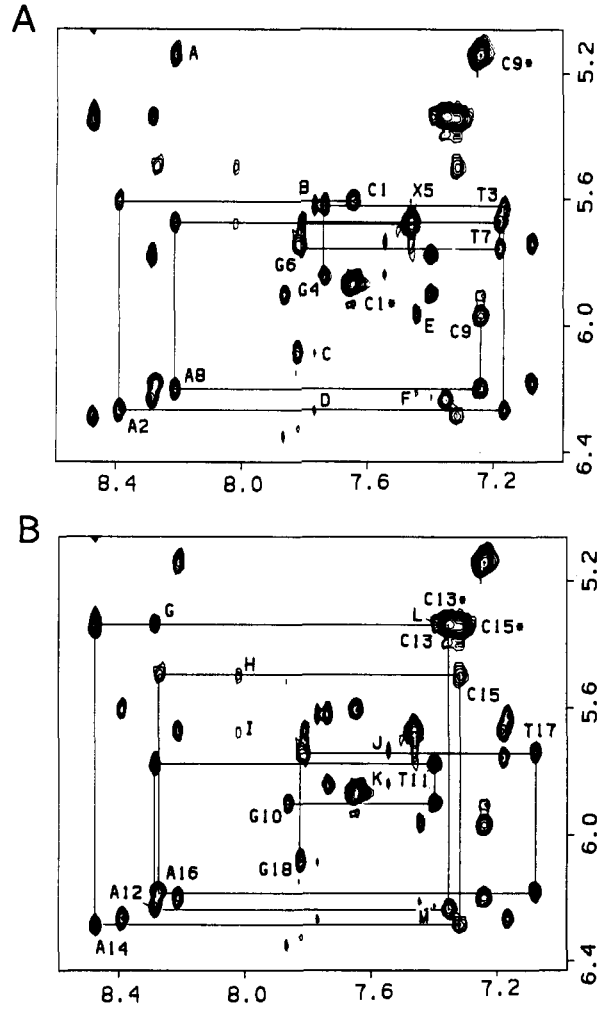

FIGURE 4: Expanded contour plots of the phase-sensitive NOESY spectrum (mixing time 250 ms) of the X·A 9-mer duplex in 0.1 M NaCl, 10 mM phosphate, and D_2O, pH 5.8 at 15 °C, establishing distance connectivities between the base protons (7.0–8.6 ppm) and the sugar H1′ and deoxycytidine H5 protons (5.0–6.4 ppm). The chain is traced from C1 to C9 in (A), and the chain is traced from G10 to G18 in (B). The tracing follows connectivities between adjacent base protons through their intervening sugar H1′ protons. The deoxycytidine H5–H6 connectivities are designated by asterisks. The assignments of NOE cross peaks A–M are (A) A8-H8 to C9-H5, (B) A2-H2 to T3-H1′, (C) A2-H2 to G18-H1′, (D) A2-H2 to A2-H1′, (E) A8-H2 to C9-H1′, (F) A8-H2 to A12-H1′, (G) A12-H8 to C13-H5, (H) A14-H2 to C15-H1′, (I) A14-H2 to X5-H1′, (J) A16-H2 to T17-H1′, (K) A16-H2 to G4-H1′, (L) A12-H2 to C13-H1′, (M) A12-H2 to A12-H1′.

NOEs to the H8 proton of flanking G4 (cross peaks in boxed regions in Figure 6A) but not to the H8 proton of flanking G6 in the X·A 9-mer.

Phosphorus Resonances. The proton-decoupled phosphorus spectrum of the X·A 9-mer in D_2O buffer, pH 5.8, at 15 °C is plotted in Figure 1C. The majority of the phosphorus resonances are dispersed between −4.0 and −4.6 ppm with one phosphorus resonance shifted downfield to −3.65 ppm (Figure 1C). This downfield shift is indicative of a perturbation in the backbone at this phosphodiester linkage. This phosphorus resonance has been assigned by correlating the known sugar proton assignments to the O3′- and O5′-linked phosphorus resonances through a heteronuclear phosphorus (observe)–proton RELAY COSY experiment on the X·A 9-mer duplex in D_2O buffer at 15 °C (positive contour levels only, Figure 7A). This experiment permits assignment of the −3.65 ppm downfield shifted phosphorus resonance to the C13pA14 phosphodiester linkage at the lesion site. A one-dimensional

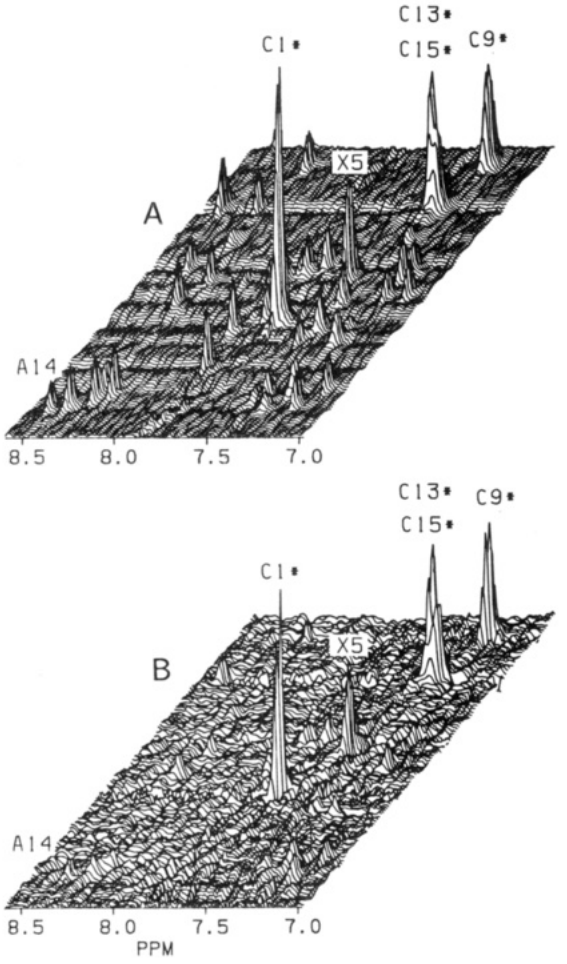

FIGURE 5: Expanded stacked plots of the phase-sensitive NOESY spectrum of the X·A 9-mer duplex in 0.1 M NaCl, 10 mM phosphate, and D_2O, pH 5.8 at 15 °C, with the cross peaks establishing distance connectivities between the base protons (7.0–8.6 ppm) and the sugar H1′ and deoxycytidine H5 protons (5.0–6.4 ppm). (A) NOESY stacked plot for 250-ms mixing time data set. (B) NOESY stacked plot for 50-ms mixing time data set. The deoxycytidine H5–H6 connectivities are designated by asterisks. The cross peak X5 corresponds to the NOE between the H8 and H1′ proton of this residue in the X·A 9-mer duplex.

slice recorded through the −3.65 ppm phosphorus resonance established the coupling connectivities to the sugar protons of C13 in the O3′-direction and to the sugar protons of A14 in the O5′-direction; this is plotted in Figure 7B.

X·G 9-mer

pH-Independent Conformation. The nonexchangeable proton NMR spectra (5.0–9.0 ppm) of the X·G 9-mer in D_2O buffer, 15 °C, have been recorded between pH 6.0 and pH 8.5. There was no indication of a pH-dependent structural transition for the X·G 9-mer duplex in contrast to what was detected for the X·A 9-mer duplex.

Exchangeable Protons. The exchangeable proton spectrum (6.0–14.0 ppm) of the X·G 9-mer duplex in H_2O buffer, pH 7.0 at 15 °C, is plotted in Figure 8A. The deoxyguanosine and thymidine imino protons are detected between 12.5 and 13.7 ppm. The exchangeable resonance at 10.5 ppm (Figure 8A) has been assigned to the imino proton of G14 at the X5·G14 lesion site. This resonance exhibits NOEs to the imino protons of flanking G4·C15 and G6·C13 base pairs (boxed region, Figure 8B) in the NOESY spectrum of the X·G 9-mer duplex in H_2O buffer, pH 7.0, 0 °C.

The chemical shifts of the imino and amino protons and deoxyadenosine H2 protons in the X·G 9-mer duplex in H_2O buffer at 0 °C are listed in Table II.

Table II: Proton Chemical Shifts in X·G 9-mer Duplex, pH 7.0

	exchangeable proton chemical shifts (ppm), 0 °C				
base pair	T-H3	G-H1	C-H4b	C-H4e	A-H2
C1·G18		12.79	8.12	7.00	
A2·T17	13.68				7.78
T3·A16	13.53				7.55
G4·C15		12.63	8.06	6.41	
X5·G14		10.60			
G6·C13		12.71	8.11	6.72	
T7·A12	13.58				7.46
A8·T11	13.64				7.49
C9·G10		12.71	8.11	6.72	

	nonexchangeable proton chemical shifts (ppm), 10 °C						
	H8	H2	H6	H5/CH_3	H1′	H2′,H2″	H3′
C1			7.68	5.90	5.63	2.02, 2.42	4.70
A2	8.42	7.80			6.29	2.77, 2.95	5.15
T3			7.19	1.43	5.68	2.05, 2.36	4.85
G4	7.79				5.78	2.58, 2.83	4.94
X5	7.22				5.72	2.58, 3.12	4.94
G6	7.54				5.76	2.43, 2.63	
T7			7.20	1.37	5.73	2.06, 2.42	
A8	8.26	7.55			6.24	2.65, 2.86	5.00
C9			7.26	5.15	6.01	2.10, 2.14	
G10	7.91				5.94	2.64, 2.77	4.81
T11			7.43	1.38	5.75	2.23, 2.53	
A12	8.31	7.50			6.24	2.71, 2.91	5.04
C13			7.08	5.24	5.61	1.42, 2.08	4.71
G14	7.93				5.68	2.58, 2.68	4.97
C15			7.45	5.31	5.67	2.13, 2.43	4.84
A16	8.34	7.59			6.24	2.71, 2.92	5.02
T17			7.12	1.49	5.77	1.86, 2.30	4.83
G18	7.86				6.11	2.23, 2.59	4.66

Nonexchangeable Protons. The NOESY spectrum (250-ms mixing time) of the X·G 9-mer duplex in D_2O buffer, pH 7.0 at 10 °C, exhibits well-resolved cross peaks that allow us to unequivocally assign the resonances for the nonexchangeable base and sugar protons. These assignments are listed in Table II. The contour plot in Figure 9A establishes distance connectivities between the base protons (7.0–8.5 ppm) and the sugar H1′ and deoxycytidine H5 protons (4.8–6.4 ppm). The H8 proton of X5 resonates at 7.22 ppm in the X·G 9-mer duplex (Table II), upfield of the other deoxyguanosine H8 protons in the duplex. This upfield shift is similar to that detected in the X·A 9-mer duplex (Table I). The base to their own H1′ proton NOE cross peaks for T3, X5, and T7 are superpositioned (Figure 9A) so that it is not possible to differentiate rigorously the NOE contribution of X5 from T3 and T7 in the X·G 9-mer duplex.

Furthermore, a stacked plot of the base proton (7.0–8.5 ppm) to sugar H1′ and deoxycytidine H5 proton (4.8–6.4 ppm) regions in the NOESY spectra of the X·G 9-mer at 250-ms (Figure 10A) and 50-ms (Figure 10B) mixing times establishes that the overlapping cross peak which includes the NOE between the H8 of X5 and its own sugar H1′ (designated X5, Figure 10) exhibits an intensity that is approximately 0.7 the intensity of the cross peaks between the H6 and H5 of deoxycytidines (designated C*, Figure 10).

The expanded NOESY contour plot establishing distance connectivities between the base protons (7.0–8.5 ppm) and the sugar H2′,2″ protons, thymidine CH_3 and exocyclic CH_2 protons (1.2–3.5 ppm) in the X·G 9-mer duplex, pH 7.0 at 10 °C, is plotted in Figure 9B. The H8 proton of G14 exhibits NOEs to its own and 5′-flanking C13 sugar H2′,2″ protons. By contrast, the H8 of X5 exhibits NOEs to its own sugar H2′,2″ protons but not to the 5′-flanking G4 sugar H2′,2″ protons (Figure 9B). Furthermore, as was observed with the

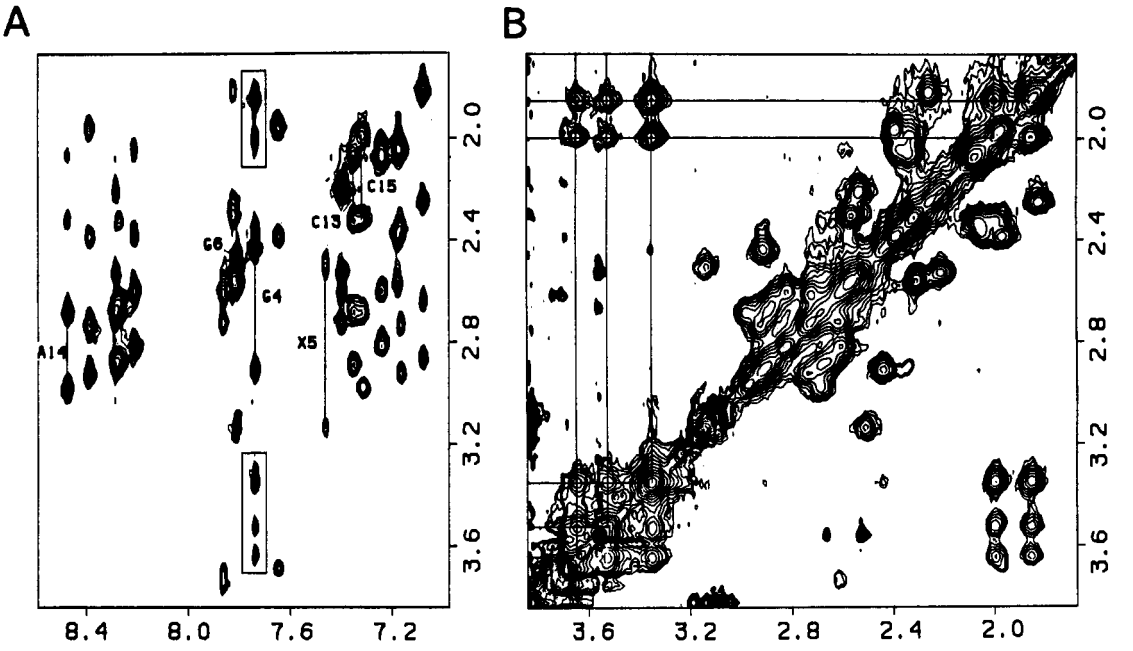

FIGURE 6: Expanded contour plots of the phase-sensitive NOESY spectra (mixing time 250 ms) of the X·A 9-mer duplex in 0.1 M NaCl, 10 mM phosphate, and D_2O, pH 5.8 at 15 °C. (A) Cross peaks establishing connectivities between the base protons (7.0–8.6 ppm) and the sugar H2′,2″ and exocyclic CH_2 protons (1.6–3.8 ppm). (B) Cross peaks establishing connectivities between sugar H2′,2″ protons and between exocyclic CH_2 protons in the symmetrical 1.6–3.8 ppm region.

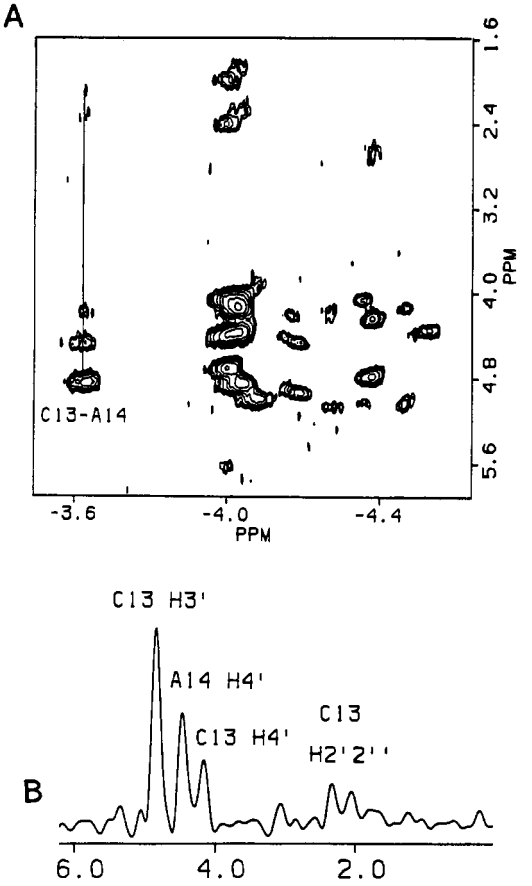

FIGURE 7: (A) Two-dimensional heteronuclear phosphorus (observe)–proton RELAY COSY contour plot of the X·A 9-mer in D_2O buffer, pH 5.8, at 15 °C. Only positive contour levels are plotted in the interest of clarity. (B) Slice recorded through the positive contour levels of the −3.65 ppm ^{31}P resonance exhibiting direct and relay connectivities to the sugar protons in both directions.

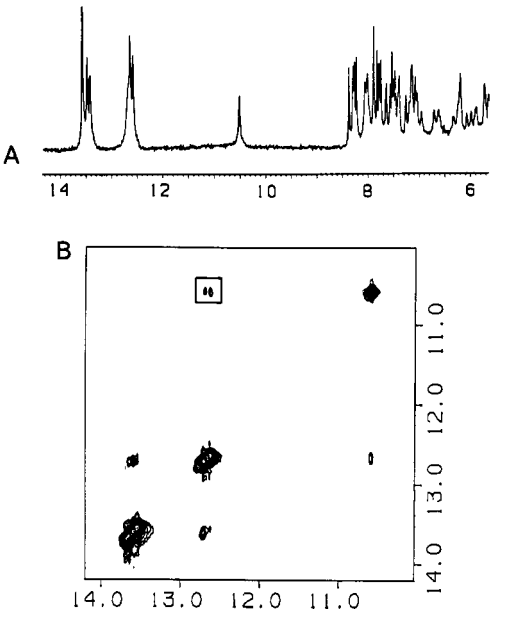

FIGURE 8: (A) 500-MHz proton NMR spectrum (5.5–14.0 ppm) of the X·G 9-mer duplex in 0.1 M NaCl, 10 mM phosphate, and H_2O, pH 7.0 at 15 °C. (B) Expanded phase-sensitive NOESY (120-ms mixing time) contour plot of the X·G 9-mer in H_2O buffer, pH 7.0, 0 °C, establishing distance connectivities between imino protons in the symmetrical 10.0–14.0 ppm region.

X·A 9-mer duplex, the exocyclic CH_2 protons at ~1.85 ppm and at 3.20–3.30 ppm exhibit NOEs to the H8 proton of flanking G4 (cross peaks in boxed region of Figure 9B) but not to the H8 proton of flanking G6 in the X·G 9-mer duplex.

Discussion

NMR studies on the X·A 9-mer duplex at acidic pH and on the X·G 9-mer duplex at neutral pH offer substantial information regarding the conformation and base-pairing possibilities at the sites of exocyclic lesion in DNA helices. We reasoned that the bulky 1,N^2-propano adduct of deoxyguanosine **2** could be readily accommodated into the helix if this base adopted a syn glycosidic torsion angle resulting in the bulky propano bridge being directed into the major groove. Our laboratory has recently demonstrated formation of a

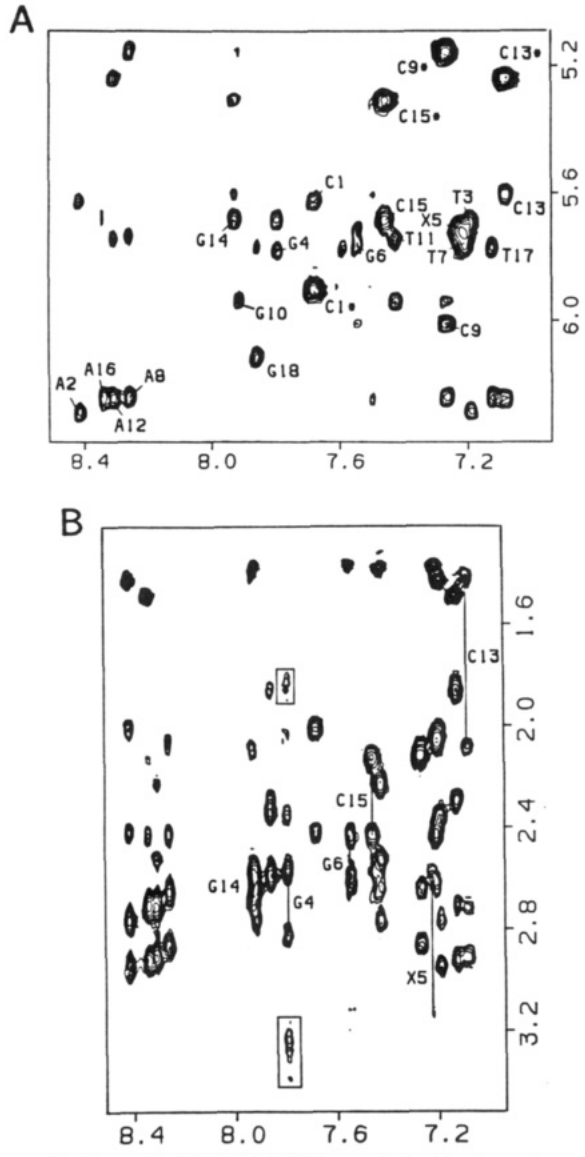

FIGURE 9: Expanded NOESY (300-ms mixing time) contour plots establishing distance connectivities (A) between the base proton (6.9–8.5 ppm) and the sugar H1′ and deoxycytidine H5 protons (4.8–6.4 ppm) and (B) between the base protons (7.0–8.5 ppm) and the sugar H2′,2″ protons, thymidine CH_3, and exocyclic CH_2 protons (1.2–3.6 ppm) in the X·G 9-mer duplex in 0.1 M NaCl, 10 mM phosphate, and D_2O, pH 7.0 at 10 °C. The H5–H6 deoxycytidine NOE connectivities are designated by asterisks. The base to their own sugar proton NOE connectivities are also assigned for individual residues in the X·G 9-mer duplex.

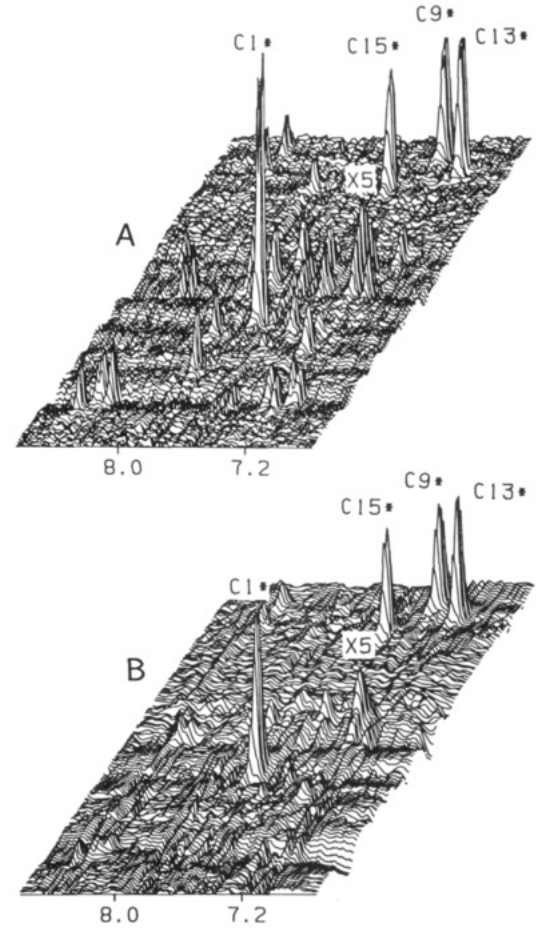

FIGURE 10: Expanded stacked plots of the phase-sensitive NOESY spectrum of the X·G 9-mer duplex in 0.1 M NaCl, 10 mM phosphate, and D_2O, pH 7.0, with the cross peaks establishing distance connectivities between the base protons (7.0–8.6 ppm) and the sugar H1′ and deoxycytidine H5 protons (5.0–6.4 ppm). (A) NOESY stacked plot for 300-ms mixing time data set at 10 °C. (B) NOESY stacked plot for 50-ms mixing time data set at 15 °C. The deoxycytidine H5–H6 connectivities are designated by asterisks. The cross peak X5 corresponds to the NOE between the H8 and H1′ protons of this residue in the X·G 9-mer duplex.

protonated G(syn)·A(anti) mismatch pair at acidic pH (Gao & Patel, 1988), and this result guided us to probe for potential protonated X(syn)·A(anti) pair formation in the X·A 9-mer duplex **3** at acidic pH. Similarly, the demonstration of a O^6CH_3G(syn)·G(anti) pair (Patel et al., 1986) and a G(syn)·G(anti) mismatch pair (Henderson et al., 1987; C. De los Santos and D. J. Patel, unpublished data) provided models for potential X(syn)·G(anti) pair formation in the X·G 9-mer duplex **4**.

The present NMR studies were undertaken with the eventual goal of defining structural features of both the X·A and X·G exocyclic adduct sites and of the flanking base pairs in solution. Our approach toward this goal was to assign initially the majority of the base and sugar proton resonances on both strands of the complementary X·A 9-mer and X·G 9-mer duplexes in H_2O and D_2O solution. Structural features of the duplex centered about the exocyclic lesion site can then be reconstructed from NOE-based distance constraints between proton pairs separated by <5 Å.

X·A 9-mer Duplex

Watson–Crick Base Pairing. The base-pairing characteristics at the exocyclic lesion and flanking regions can be probed by recording the imino proton spectra and monitoring NOE connectivities involving imino protons and protons across the base pair. The four thymidine imino protons are resolved in the X·A 9-mer duplex, pH 5.8 at 15 °C (Figure 1A), and each exhibits NOEs to deoxyadenosine H2 protons across the base pair (Figure 2B) consistent with formation of Watson–Crick A2·T17, T3·A16, T7·A12, and A8·T11 base pairs. The two nonterminal deoxyguanosine imino protons are also well resolved (Figure 1A), and each exhibits NOEs to deoxycytidine amino protons across the pair (Figure 2B) consistent with formation of Watson–Crick G4·C15 and G6·C13 base pairs. These results establish the presence of intact G·C base pairs on either side of the exocyclic X·A site in the X·A 9-mer duplex, pH 5.8, 15 °C.

Helix Handedness and Base Stacking. The NOE cross peaks observed in the NOESY spectra of the X·A 9-mer duplex, pH 5.8, 15 °C, in H_2O (Figure 2A) and in D_2O (Figure 3A) exhibit directionality reflecting the handedness of the helix. Observed NOEs between the base (purine H8

or pyrimidine H6) protons and their own and 5'-linked sugar (H1', H2',2", and H3') protons, NOEs between adjacent base protons in purine (3'–5')pyrimidine (A2-T3, G6-T7, A8-C9, G10-T11, A12-C13, and A16-T17) steps, and NOEs between deoxyadenosine H2 protons and sugar H1' protons on the partner strand (cross peaks C, F, and K, Figure 4A,B) establish the presence of a right-handed helix with all bases being stacked into the duplex.

A14 at the Lesion Site. The NOE connectivities involving the base and sugar protons of A14 in the (G4-X5-G6)·(C13-A14-C15) segment provide structural constraints on this base located opposite the exocyclic deoxyguanosine X5 in the X·A 9-mer duplex at pH 5.8.

The observed NOEs between the H8 proton of A14 to its own sugar H1' and H2',2" protons and to those of flanking C13 (Figures 4B and 6A) establish that A14 is stacked in a right-handed C13-A14-C15 segment. The weak NOE between the H8 proton of A14 and its own sugar H1' proton relative to the strong NOE between the H6 and H5 protons of deoxycytidine in NOESY spectra (50-ms mixing time) (Figure 5B) is consistent with an anti glycosidic torsion angle at A14 in the X·A 9-mer duplex, pH 5.8.

The amino protons of A14 in the X·A 9-mer duplex, pH 5.8 at 15 °C, resonate at 10.18 and 8.28 ppm (Figure 1A) and have been identified by the strong NOE between them (box C, Figure 2A) characteristic of geminal protons and the observed NOE between the 10.18 ppm amino proton of A14 and the imino protons of flanking G4·C15 and G6·C13 base pairs (box D, Figure 2A) in the X·A 9-mer duplex. The positions of the hydrogen-bonded (10.18 ppm) and exposed (8.28 ppm) amino protons of A14 in the X·A 9-mer duplex at pH 5.8 are approximately 2 ppm downfield from the hydrogen-bonded (8.0–8.5 ppm) and exposed (6.5–7.0 ppm) amino protons of deoxyadenosine in unperturbed helices. These data suggest that the A14 ring is protonated at the X5·A14 lesion site. Similar downfield chemical shifts for amino protons in protonated deoxyadenosine bases have been reported for the protonated G(syn)·A(anti) mismatch pair in DNA (Gao & Patel, 1988).

It should be noted that the H8 proton of A14 resonates at 8.47 ppm and is the most downfield of the five deoxyadenosine H8 protons in the X·A 9-mer duplex, pH 5.8 (Table I). This downfield shift is indicative of protonation of A14 at the X5·A14 lesion site and is consistent with a similar downfield shift for the deoxyadenosine H8 proton reported for the protonated G(syn)·A(anti) mismatch pair in DNA helices (Gao & Patel, 1988).

We have been unable to detect the proton involved in N1 protonation of A14 in the X·A 9-mer duplex, pH 5.8 at 15 °C, and this must reflect its rapid exchange characteristics.

X5 at the Lesion Site. Structural features of the 1,N^2-propanodeoxyguanosine X5 lesion have been defined from intranucleotide and internucleotide NOEs in the (G4-X5-G6)·(C13-A14-C15) segment of the X·A 9-mer duplex at pH 5.8.

The NOE detected between the H8 base proton and its own sugar H1' proton for X5 is more intense than the corresponding NOEs for all the other deoxynucleotides in the NOESY spectra recorded at 250-ms (Figure 5A) and 50-ms (Figure 5B) mixing times. This observation requires that there be a perturbation at the glycosidic torsion angle of X5 relative to anti glycosidic torsion angles, which are present for all other residues in the X·A 9-mer duplex at pH 5.8. The NOE cross-peak intensity between the H8 and H1' protons of X5 is approximately 0.7 the intensity of the NOEs between the H6 and H5 protons of deoxycytidines (fixed separation of 2.45 Å) in the X·A 9-mer duplex (Figure 5A,B). The NOE is inversely dependent on the sixth power of the interproton distance so that this translates into an interproton separation of ~2.6 Å between the H8 and H1' protons of X5. This same separation would be ~2.6 Å for a syn glycosidic torsion angle orientation and ~3.7 Å for an anti glycosidic torsion angle orientation (Patel et al., 1982b). We conclude that X5 adopts a syn glycosidic torsion angle in the X·A 9-mer duplex at pH 5.8.

The 7.46 ppm chemical shift of the H8 proton of X5 is the most upfield of all the purine H8 protons in the X·A 9-mer duplex at pH 5.8 (Table I). This can be accounted for by the close proximity of the H8 proton over the aromatic rings of the flanking base pairs when X5 assumes the syn orientation about the glycosidic bond. A similar upfield shift has been detected for the H8 proton of deoxyguanosine at the protonated G(syn)·A(anti) mismatch pair in DNA helices (Gao & Patel, 1988).

The formation of a syn glycosidic torsion angle at X5 results in alterations in distance connectivities between the H8 proton of X5 and sugar protons of the 5'-flanking G4 residue in the X·A 9-mer duplex at pH 5.8. Thus, we do not detect NOE cross peaks between the H8 proton of X5 and the H1' proton of G4 (Figure 4A) and the H2',2" proton of G4 (Figure 6A). Similarly, the H8 proton of O^6meG does not exhibit NOEs to the sugar protons of its 5'-flanking residue at the O^6meG-(syn)·G(anti) lesion site in a DNA helix (Patel et al., 1986).

The imino proton of deoxyguanosine is lost on formation of 1,N^2-propanodeoxyguanosine, and we have not detected the substituted amino proton at the 2-position of 1,N^2-propanodeoxyguanosine in the X·A 9-mer duplex, pH 5.8 at 15 °C. By contrast, all CH_2 protons on the exocyclic propano ring of X5 can be identified by distance connectivities in the NOESY spectra (box D, Figure 3A). The exocyclic bridge of 1,N^2-propanodeoxyguanosine is located in the major groove for X5, which is in the syn glycosidic bond orientation range, and we detect NOEs between all CH_2 protons and the major groove H8 protons of G4 but not of G6 in the G4-X5-G6 segment (boxed regions, Figure 6A). The observed directionality of the NOEs between major groove protons on adjacent bases must reflect the right-handedness of the helix centered about the X5 lesion site in the X·A 9-mer duplex.

Protonated X5(syn)·A14(anti) Pairing. The above NMR data and analysis establish that X5 is syn and A14 is anti at the X5·A14 lesion site and that A14 is protonated in the X·A 9-mer duplex at pH 5.8. The resulting protonated X5-(syn)·A14(anti) pair stabilized by two hydrogen bonds brings the H8 proton of X5 and the H2 proton of A14 in close proximity as shown in **5**. Experimentally, the observation of an NOE between the H8 of X5 and the H2 of A14 (boxed cross peak, Figure 3B) confirms this alignment in the X·A 9-mer duplex at pH 5.8. A similar NOE was detected between the H8 of deoxyguanosine and H2 deoxyadenosine at the protonated G(syn)·A(anti) mismatch site in a DNA helix (Gao & Patel, 1988).

X·G 9-mer

Base Pairing and Helix Handedness. The NMR parameters establish that all A·T and G·C pairs including G4·C15 and G6·C13 which flank the X5·G14 lesion site adopt Watson–Crick pairing in the X·G 9-mer at neutral pH. The observed NOEs between the 10.5 ppm imino proton of G14 and the imino protons of flanking G4·C15 and G6·C13 base pairs establish that G14 is stacked into the helix (anti glycosidic torsion angle) between intact flanking base pairs in the X·G

9-mer duplex (boxed cross peaks, Figure 8B). The observed directionality of the NOEs between nonexchangeable base and sugar protons for the X·G 9-mer duplex (Figure 9A) demonstrates formation of a right-handed helix in aqueous solution.

X5·G14 Lesion Site. The H8 proton of G14 exhibits NOEs to its own H1′ and H2′,2″ protons and to those of its 5′-flanking C13 residue consistent with an anti glycosidic torsion angle at G14 in the X·G 9-mer duplex. By contrast, the overlap of the chemical shifts of the H8 proton of X5 and the H6 protons of T3 and T7 at ~7.21 ppm and the H1′ protons of T3, X5, and T7 at ~5.71 ppm limits the conclusions that can be deduced about the orientation of the X5 residue (Figure 9A).

However, we do note similarities between the NMR chemical shift and NOE parameters for X5 at the X5·A14 lesion site in the X·A 9-mer duplex at pH 5.8 and at the X5·G14 lesion site in the X·G 9-mer duplex at pH 7.0. Thus, the H8 proton of X5 (7.46 ppm, Table I) in the X·A 9-mer duplex and the H8 proton of X5 (7.22 ppm, Table II) in the X·G 9-mer duplex are at the highest field of all purine H8 protons. Furthermore, the expanded stacked NOESY plots at 250- and 50-ms mixing times exhibit similar ratios in the relative intensities of the peaks labeled X5 (H8 of X5 to H1′ of X5) and C9* (H6 of C9 to H5 of C9) for the X·A 9-mer duplex at pH 5.8 (Figure 5) and the X·G 9-mer duplex at pH 7.0 (Figure 10).

Furthermore, the H8 proton of X5 does not exhibit NOEs to the sugar H2′,2″ protons of 5′-flanking G4 in both the X·A 9-mer duplex, pH 5.8 (Figure 6A), and the X·G 9-mer duplex, pH 7.0 (Figure 9B). The observed NOEs between the exocyclic CH_2 protons and the H8 proton of G4 but not between the H8 proton of G6 in the X·G 9-mer duplex, pH 7.0 (Figure 9B), parallels similar observations in the X·A 9-mer duplex at pH 5.8 (Figure 6A), thus displaying further similarities in structural features at the lesion site in the two duplexes.

X5(syn)·G14(anti) Pairing. The above results are consistent with a X5(syn)·G14(anti) pairing orientation **6** at the lesion

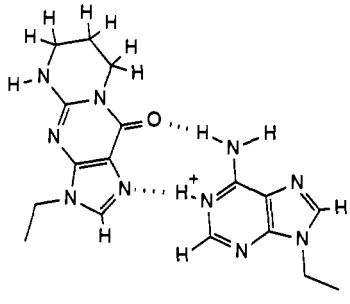

5

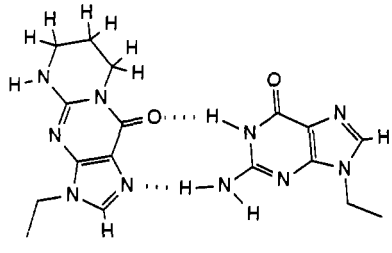

6

site for the X·G 9-mer duplex at pH 7.0 and may be compared to the protonated X5(syn)·A14(anti) pairing **5** established for the X·A 9-mer duplex at pH 5.8. It should be noted that A14(anti) uses its N^1-protonated imino and N^6-amino positions to pair with X5(syn) in the proposed protonated X5(syn)·A14(anti) pairing alignment **5** while G14(anti) uses its N^1-imino and N^2-amino positions to pair with X5(syn) in the proposed X5(syn)·G14(anti) pairing alignment **6**.

The imino proton of G14 at the X5·G14 lesion site resonates at 10.6 ppm in the X·G 9-mer duplex (Figure 8A) and is upfield from the imino proton of Watson–Crick base pairs (12.5–13.5 ppm). This upfield shift probably reflects formation of an imino NH–carbonyl hydrogen bond in the X5(syn)·G14(anti) pair **6** compared to an imino NH–ring nitrogen hydrogen bond in a Watson–Crick pair. It should be noted that deoxyguanosine imino NH–carbonyl hydrogen bonds in wobble G·T mismatches in DNA resonate in the 10.5 ppm region (Patel et al., 1982a).

Biological Implications. The central reaction in the biosynthesis of DNA involves the enzymatic polymerization of nucleotide triphosphates on a single-strand DNA template. Alterations in base-pairing properties of this template could lead to misincorporation of nucleotides and, possibly, to mutagenesis. The NMR studies reported in this paper demonstrate that a stable right-handed duplex DNA structure can be formed at pH 5.8 when the exocyclic adduct, 1,N^2-propanodeoxyguanosine, adopts the syn conformation and dG or dA residues located opposite the lesion are in the anti configuration. If a similar pattern of base pairing occurs during enzymatic DNA synthesis, G → T and/or G → C transversions should occur at the site of the modified base. Biological experiments have been undertaken to test this prediction.

Summary. The results and interpretations presented in these NMR studies provide the first insights into the pairing of exocyclic ring modified bases at the oligodeoxynucleotide level. The particular examples under study involved the pairing of 1,N^2-propanodeoxyguanosine (**2**) with the purine bases deoxyadenosine and deoxyguanosine located in the center of complementary nonadeoxynucleotides in aqueous solution. The application of two-dimensional NMR methods to the exocyclic lesion contained in DNA oligomers provides spectral resolution at the individual base pair level with the ability to monitor exchangeable and nonexchangeable protons distributed throughout each deoxynucleotide unit in the duplex.

The NMR studies on the X·A 9-mer duplex **3** demonstrate the existence of distinct conformations at the X·A lesion site at pH 5.8 and pH 8.9 and emphasize the importance of pH in modulating conformational equilibria. The present paper addresses the structural basis for the low-pH response by defining the pairing at the X5·A14 lesion site in the X·A 9-mer duplex at pH 5.8. Steric constraints across the lesion site define the nature of the pairing interaction between two purines, one of which contains an exocyclic adduct across the normal Watson–Crick hydrogen-bonding edge. The NMR studies on the X·A 9-mer at pH 5.8 demonstrate that this problem is resolved through formation of a protonated X5(syn)·A14(anti) pair at the lesion at acidic pH.

The formation of a syn configuration at the X5 glycosidic bond is readily identified from the magnitude of the observed NOE between the H8 proton of X5 and its own sugar H1′ proton and is supported by the unusual upfield shift of the H8 proton of X5 at the lesion site. The exocyclic ring is directed into the major groove in the X5(syn) orientation, and the modified base uses Hoogsteen-type pairing with deoxyadenosine on the partner strand. The observed distance connectivities between the exocyclic CH_2 protons of X5 and the H8 proton of flanking G4 but not of flanking G6 located in the major groove establish that the helix retains its right-handedness. The magnitude of the H8 proton to H1′ proton

NOE at A14 demonstrates that this base adopts an anti configuration at its glycosidic bond. The large downfield shift of ~2 ppm at the 6-amino protons and a smaller downfield shift at the H8 proton of A14 establish protonation of the A14 base.

Pairing at the protonated X5(syn)·A14(anti) lesion site is stabilized by two hydrogen bonds as a result of ring protonation with the alignment drawn in **5**. This alignment is confirmed by the observation of a critical NOE in the minor groove between the H8 of X5 and the H2 of A14 in the X·A 9-mer duplex at pH 5.8. These results for pairing at an exocyclic deoxyguanosine adduct opposite deoxyadenosine at low pH represent a logical extension of the recent demonstration of protonated G(syn)·A(anti) mismatch pair formation at low pH (Gao & Patel, 1988). We observe a downfield shift of the C13-A14 phosphorus resonance in the X·A 9-mer duplex that presumably reflects a perturbation in the phosphodiester backbone at this position associated with accommodation of the X5·A14 lesion into the DNA helix.

NMR studies were also conducted in parallel on the pairing of the X5·G14 lesion in the X·G 9-mer duplex **4**. The NMR spectral parameters were independent of pH between pH 6.0 and pH 8.5 and are consistent with X5(syn)·G14(anti) pairing **6** stabilized by two hydrogen bonds at the lesion site in the X·G 9-mer duplex at neutral pH. This research extends earlier contributions that demonstrated O^6meG(syn)·G(anti) pairing at an O-alkylation site (Patel et al., 1986) and G(syn)·G(anti) pairing at a purine·purine mismatch site (Henderson et al., 1987; de los Santos and Patel, unpublished results) in DNA helices.

The present contribution and earlier research emphasize the importance of the syn glycosidic torsion angle at purines and ring protonation at low pH in the formation of base pairs stabilized by two hydrogen bonds that could otherwise not be accomodated into the DNA helix without major structural perturbations.

ACKNOWLEDGMENTS

NMR studies were conducted on instruments purchased with funds provided by the Robert Woods Johnson, Jr., Charitable Trust and the Matheson Foundation. We acknowledge extensive discussions with our collaborator Dr. M. Eisenberg of the Department of Pharmacological Sciences, SUNY, Stony Brook, who is modeling the incorporation of exocyclic adducts into DNA using molecular dynamics computations guided by NMR-based distance constraints. We also acknowledge helpful discussions with Dr. Michael Zagorski, Dr. David Norman, and Matthew Kalnik in the NMR laboratory.

Registry No. **2**, 120667-07-4; **2** 5′-*O*-(dimethoxytrityl) derivative, 120667-13-2; **2** 5′-*O*-(dimethoxytrityl) and 3′-*O*-(β-cyanoethyl *N*,*N*-diisopropylphosphoramidite derivative), 120667-14-3; **3**, 120667-10-9; **4**, 120667-12-1; 1,3-dibromopropane, 109-64-8; 2′-deoxyguanosine, 961-07-9; deoxyadenosine, 958-09-8.

REFERENCES

Basu, A. K., & Essigmann, J. M. (1988) *Chem. Res. Toxicol. 1*, 1–18.

Chung, F. L., Young, R., & Hecht, S. S. (1984) *Cancer Res. 44*, 990–995.

Gao, X., & Patel, D. J. (1988) *J. Am. Chem. Soc. 110*, 5178–5182.

Hare, D. R., Wemmer, D. E., Chou, S. H., Drobny, G., & Reid, B. R. (1983) *J. Mol. Biol. 171*, 319–336.

Henderson, E., Hardin, C. C., Walk, S. K., Tinoco, I., Jr., & Blackburn, E. H. (1987) *Cell 51*, 899–908.

Hore, P. J. (1983) *J. Magn. Reson. 55*, 283–300.

Kalnik, M. W., Chang, C. N., Grollman, A. P., & Patel, D. J. (1988) *Biochemistry 27*, 924–931.

Otting, G., Widmer, H., Wagner, G., & Wüthrich, K. (1985) *J. Magn. Reson. 66*, 187–193.

Patel, D. J., Kozlowski, S. A., Marky, L. A., Rice, J. A., Broka, C., Dallas, J., Itakura, K., & Breslauer, K. J. (1982a) *Biochemistry 21*, 437–444.

Patel, D. J., Kozlowski, S. A., Nordheim, A., & Rich, A. (1982b) *Proc. Natl. Acad. Sci. U.S.A. 79*, 1413–1417.

Patel, D. J., Shapiro, L., Kozlowski, S. A., Gaffney, B. L., & Jones, R. A. (1986) *J. Mol. Biol. 188*, 677–692.

Patel, D. J., Shapiro, L., & Hare, D. R. (1987) *Q. Rev. Biophys. 20*, 35–112.

Reid, B. R. (1987) *Q. Rev. Biophys. 20*, 1–34.

Shapiro, R. (1969) *Ann. N.Y. Acad. Sci. 163*, 624–630.

Singer, B., & Grunberger, D. (1983) in *Molecular Biology of Mutagens and Carcinogens*, Plenum Press, New York.

Singer, B., & Bartsch, H. (1986) *The Role of Cyclic Nucleic Acid Adducts in Carcinogenesis and Mutagenesis*, IARC Scientific Publications 70, International Agency for Research on Cancer, Lyon, France.

Takeshita, M., Chang, C. N., Johnson, F., Will, S., & Grollman, A.P. (1987) *J. Biol. Chem. 262*, 10171–10179.

Van de Ven, F. J., & Hilbers, C. W. (1988) *Eur. J. Biochem. 178*, 1–38.